







RESEARCH ARTICLE | NOVEMBER 01 2023

Electron-enhanced atomic layer deposition of Ru thin films using Ru(DMBD)(CO)₃ and effect of forming gas anneal

Michael A. Collings ; Marcel Junige ; Andrew S. Cavanagh ; Victor Wang ; Andrew C. Kummel ; Steven M. George 



J. Vac. Sci. Technol. A 41, 062408 (2023)

<https://doi.org/10.1116/6.0002938>



View
Online



Export
Citation

CrossMark



Instruments for Advanced Science

- Knowledge
- Experience
- Expertise

Click to view our product catalogue

Contact Hiden Analytical for further details:

www.HidenAnalytical.com

info@hiden.co.uk

Gas Analysis

- dynamic measurement of reaction gas streams
- catalysis and thermal analysis
- molecular beam studies
- dissolved species probes
- fermentation, environmental and ecological studies

Surface Science

- UHV TPD
- SIMS
- end point detection in ion beam etch
- elemental imaging - surface mapping

Plasma Diagnostics

- plasma source characterization
- etch and deposition process reaction kinetic studies
- analysis of neutral and radical species

Vacuum Analysis

- partial pressure measurement and control of process gases
- reactive sputter process control
- vacuum diagnostics
- vacuum coating process monitoring







Electron-enhanced atomic layer deposition of Ru thin films using Ru(DMBD)(CO)₃ and effect of forming gas anneal

Cite as: J. Vac. Sci. Technol. A 41, 062408 (2023); doi: 10.1116/6.0002938

Submitted: 1 July 2023 · Accepted: 26 September 2023 ·

Published Online: 1 November 2023



Michael A. Collings,¹  Marcel Junige,¹  Andrew S. Cavanagh,¹  Victor Wang,²  Andrew C. Kummel,²  and Steven M. George¹ 

AFFILIATIONS

¹Department of Chemistry, University of Colorado, 215 UCB, Boulder, Colorado 80309-0215

²Department of Chemistry & Biochemistry, University of California San Diego, La Jolla, California 92093-0332

Note: This paper is part of the 2024 Special Topic Collection on Atomic Layer Deposition (ALD).

ABSTRACT

Ruthenium (Ru) thin films were deposited utilizing electron-enhanced atomic layer deposition (EE-ALD). Sequential exposures of Ru(DMBD)(CO)₃ (DMBD = 2,3-dimethylbutadiene) and low-energy electrons at ~125 eV were used to grow the Ru films at temperatures ≤160 °C. The electrons were obtained from a hollow cathode plasma electron source that provided an electron current of ~200 mA over a surface area of ~4 cm². Low-energy electrons can desorb surface ligands derived from Ru(DMBD)(CO)₃, such as CO, through electron-stimulated desorption. The desorbed surface ligands leave chemically reactive sites for subsequent Ru(DMBD)(CO)₃ precursor adsorption. Ru EE-ALD film growth was monitored utilizing *in situ* spectroscopic ellipsometry (SE). The electron exposures resulted in rapid Ru film nucleation and growth. Under saturation conditions at 160 °C, the growth rate for Ru EE-ALD was 0.2 Å/cycle. The electron efficiency factor for Ru EE-ALD was ~21 500 electrons/deposited Ru atom. There was no film growth without electron exposures. Ru growth was observed on various substrates including silicon with native oxide and titanium. Ru growth was also obtained on insulating substrates such as 400 nm thick thermal SiO₂ substrates. XPS analysis measured <1 at. % oxygen in the deposited Ru films. XRD, x-ray reflectivity, and SE were used to characterize the Ru films before and after forming gas anneal (FGA). FGA successfully removed carbon impurities from the as-deposited Ru films. The resistivity of the Ru EE-ALD films after FGA was determined to be as low as 17 μΩ cm for a film thickness of 6.7 nm. SE measurements of the imaginary part of the pseudodielectric function, ⟨ε₂⟩, were utilized to characterize the as-deposited Ru films and the high purity Ru films after FGA. The low resistivity of the Ru films after FGA was consistent with a prominent Drude absorption in the ⟨ε₂⟩ spectrum at ≤1 eV. Various reactive background gases such as H₂, NH₃, and H₂O were utilized during EE-ALD to attempt to remove the carbon from the as-deposited Ru EE-ALD films.

Published under an exclusive license by the AVS. <https://doi.org/10.1116/6.0002938>

I. INTRODUCTION

Electron-enhanced atomic layer deposition (EE-ALD) can enable thin film growth of various materials at low temperatures with precise thickness control. EE-ALD has been demonstrated to deposit GaN,¹ Si,² BN,³ Co,^{4,5} and TiN films.⁶ EE-ALD alternates sequential exposures of gas-phase reactants and electrons, typically with electron energies below 125 eV. This process is analogous to ALD when the electrons are considered a coreactant.⁷ The low-energy electrons facilitate film growth through a nonthermal electron-stimulated desorption (ESD) mechanism.⁸ ESD of surface

ligands provides open sites for precursor adsorption.⁹ Alternating between the gas-phase precursor and electron exposures can yield atomic layer control of the thin film growth at reduced temperatures.

Si growth using disilane (Si₂H₆) and electrons is a model EE-ALD system.² Si has been deposited previously using alternating exposures of disilane and electrons at low electron energies of 25–200 eV.² Hydrogen desorption via ESD was proposed as the critical step during Si EE-ALD. The desorbed hydrogen leaves silicon dangling bonds on the surface that are available for the dissociative adsorption of disilane. The resulting Si EE-ALD growth rates were 0.3 Å/cycle at room temperature.²

01 November 2023 15:24:00

Many of the previous EE-ALD experiments have been performed using an electron gun as the electron source.^{1–4} This paper utilized a hollow cathode plasma electron source (HC-PES) as the electron source.⁵ The HC-PES is robust and chemically inert, as well as able to deliver high electron currents of ~ 200 mA over a ~ 4 cm² area. This electron current is $\sim 1000\times$ higher than previous currents of ~ 200 μ A from electron guns.² The HC-PES can provide its maximum electron flux with short rise times of less than 10 ms.⁵ A particular feature of the current work is that the HC-PES was integrated into a viscous-flow ALD reactor. This viscous-flow ALD reactor is similar to the reactors employed in previous thermal ALD experiments.^{10,11} Including an HC-PES in a viscous-flow reactor allows thin films to be grown more rapidly than previous work using an HC-PES in a high vacuum chamber.⁵

Ruthenium is an emerging material for back-end interconnects. Interest in Ru is growing due to its favorable resistivity scaling at small feature sizes.¹² Ru does not require a diffusion barrier, such as TiN or TaN, that can consume a considerable volume in back-end interconnects.¹² The thermal ALD of Ru often involves oxidative coreactants.^{13–22} These oxidative coreactants can leave oxygen in the Ru film, and the oxygen can increase the film resistivity. In addition, the oxidative coreactants can lead to unwanted oxidation at the contacts of back-end interconnects.

EE-ALD is a promising deposition technique for Ru because EE-ALD enables film growth without oxidative coreactants. EE-ALD also provides topographical area selectivity that can enable the bottom-up fill of high aspect ratio features such as vias.⁵ Additionally, thermal ALD of Ru has been challenging to nucleate on oxide surfaces.^{18,19} Nucleation of Ru films using zero-valent precursors has proven to be more facile.^{21,23} EE-ALD can enable rapid nucleation resulting from the high density of reactive sites created by ESD.⁵

This paper explored Ru EE-ALD using sequential exposures of Ru(DMBD)(CO)₃ [η^4 -2,3-dimethylbutadiene(tricarbonyl)ruthenium(0)] and low-energy electrons at ~ 125 eV. The paper begins with an overview of the viscous-flow reactor used for the EE-ALD experiments. The paper then details the EE-ALD film growth, monitored by *in situ* spectroscopic ellipsometry (iSE), on both conducting and insulating substrates. EE-ALD films are further characterized before and after forming gas anneal (FGA) by x-ray photoelectron spectroscopy (XPS), variable angle spectroscopic ellipsometry (VASE), four-point probe (4PP), x-ray diffraction (XRD), atomic force microscopy (AFM), x-ray reflectivity (XRR), and energy-dispersive x-ray spectroscopy (EDXS) measurements. Finally, various reactive background gases (RBGs) are explored in an attempt to remove carbon impurities and tune the film composition.

II. EXPERIMENTAL PROCEDURE

A. EE-ALD reactor and reactants

EE-ALD experiments were conducted in a V-shaped vacuum reactor that adapted a previously reported hot-wall, viscous-flow design.^{10,11} The V-shape facilitated iSE at a nominal incident angle of 70°. Isothermal heating ensured that the sample was maintained at a similar temperature as the hot reactor walls. In addition, this reactor incorporated an HC-PES that delivered high electron

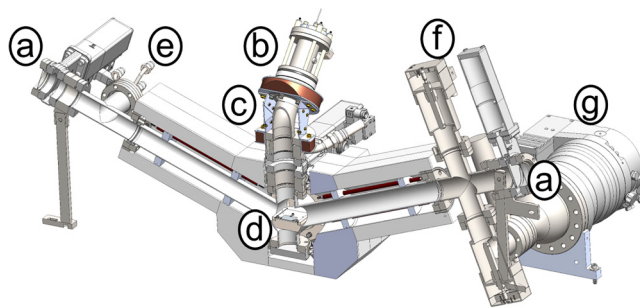


FIG. 1. Schematic of V-shaped reactor showing: (a) Windows for iSE; (b) HC-PES; (c) electron optics; (d) sample stage; (e) gas manifold inlet; (f) rough exhaust; and (g) turbomolecular pump.

currents. This apparatus implemented precursor exposures and purge steps under viscous-flow conditions at higher pressures of ~ 1 Torr in combination with electron exposures at lower pressures of ~ 1 mTorr. Figure 1 shows a schematic of this EE-ALD reactor with HC-PES.

The main reactor body was evacuated with either a rotary vane pump (Pfeiffer Pascal 2010C1) to a base pressure of ~ 1 mTorr or a turbomolecular pump (Pfeiffer HiPace 300P) to a base pressure of 5×10^{-8} Torr. The turbomolecular pump was backed by a separate rotary vane pump (Pfeiffer Pascal 2010C1). A set of valves were used to alternate between the rotary vane pump for viscous-flow precursor doses and the turbomolecular pump for electron exposures. A bypass always connected the HC-PES to the turbomolecular pump to ensure that the pressure remained low enough to maintain the HC plasma. This arrangement allowed the HC plasma to be sustained during precursor adsorption.

The chemically robust HC-PES enables a reactive background gas (RBG) to be included in the EE-ALD process.⁶ One example of using an RBG together with the HC-PES is TiN EE-ALD.⁶ An RBG can be introduced during the entire EE-ALD process. Figure 2 shows a temporal schematic of a typical EE-ALD cycle where an optional RBG (e.g., NH₃, H₂, O₂, or H₂O) can be introduced to modify the film composition. The HC-PES can operate with RBG pressures as high as a few mTorr in the reactor.

Ru(DMBD)(CO)₃ from EMD Performance Materials was used as a zero-valent Ru metalorganic precursor. Ru(DMBD)(CO)₃ has a vapor pressure of 0.5 Torr at 20 °C. Ru(DMBD)(CO)₃ was loaded into a stainless-steel cylinder and left at room temperature. Ru(DMBD)(CO)₃ has been used for thermal Ru ALD with oxidative coreactants at 160–320 °C^{21,23,24} or with nonoxidative coreactants at 200–210 °C.²⁵ In these Ru EE-ALD experiments, nitrogen (N₂, Airgas, 99.999%) was used as a carrier gas. An N₂ flow of 100 SCCM was used during reactant doses and the subsequent purge steps. Additional Ru EE-ALD experiments used Ru₃(CO)₁₂ (Sigma-Aldrich, 99%) as the Ru precursor.

Electrons were derived using an argon (Ar, Airgas 99.999%) plasma in the HC-PES.^{5,6} A voltage of -125 V on a bias grid was used to define the energy of electrons from the HC plasma. The electron current incident on the substrate and sample holder was ~ 200 mA. An accurate measurement of the electron current

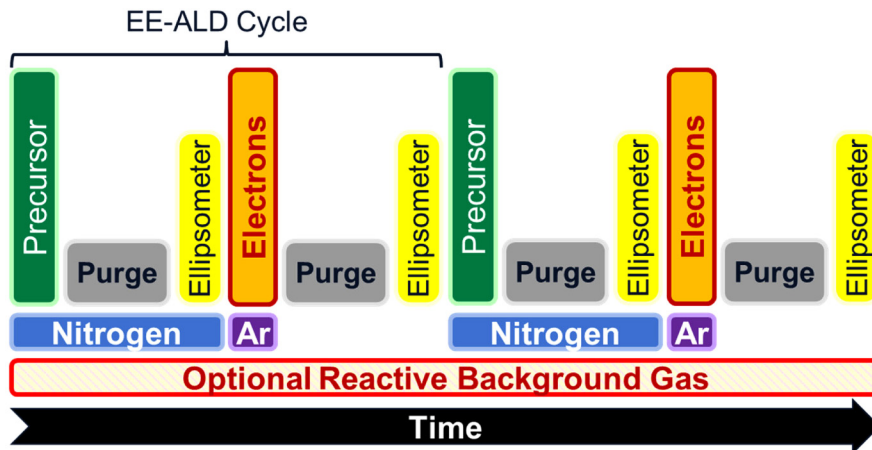
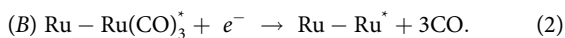
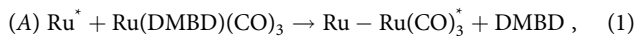


FIG. 2. Processing sequence during an EE-ALD cycle including the option of an RBG.

required a DC bias of +90 V to pull back the secondary electrons emitted from the substrate and sample holder.²⁶ The +90 V bias was applied to the substrate and sample holder using a battery in series with the current monitor. The DC bias was only used to measure the electron current and was not applied during Ru EE-ALD.

The electrons exited through a molybdenum aperture on the HC.⁵ Ar gas in the HC plasma at a pressure of ~350 mTorr also escaped through this aperture. This Ar flow through the aperture produced a constant Ar partial pressure of ~1 mTorr in the chamber. The HC plasma is also a source of sputtered atoms from the walls and aperture of the HC. Electromagnetic coils were used to steer the electron beam to remove this sputtered material from the electron beam path.⁵

EE-ALD can be separated into two individual half-reactions similar to a thermal ALD process.⁷ Ru EE-ALD using Ru(DMBD)(CO)₃ and electrons can be described as



In these equations, the asterisks denote surface species. Dissociative desorption of the DMBD ligand during initial precursor exposure on the Ru surface in step (A) has been proposed based on mass spectrometry and density functional theory (DFT) calculations.^{21,27} Studies of CO desorption kinetics from Ru(001) have shown that CO desorption from the Ru surface is slow at CO coverages <0.33 monolayer (ML), temperatures of ≤160 °C, and timescales used for the EE-ALD experiments.^{28–30} The resulting CO-terminated Ru surface is then exposed to electrons in step (B). The electrons desorb CO ligands by ESD. The desorption of CO ligands leads to a return to a Ru surface. The cycle of (A) and (B) reaction steps is then repeated to grow the Ru film.

The Ru thin film growth during EE-ALD in this study was compared with thermal ALD that utilized an FHR-ALD-300 reactor at TU Dresden.^{17,19} The thermal ALD process employed [(ethyl cyclopentadienyl)(pyrrolyl) ruthenium(II)] (ECPRu) as the

metalorganic precursor and molecular oxygen (O₂) as the coreactant at a deposition temperature of ~275 °C. Previous reports have detailed this Ru thermal ALD process.^{15–20}

B. Spectroscopic ellipsometry and substrate materials

An M-2000® spectroscopic ellipsometer (J.A. Woollam Co., Inc.) was used to monitor EE-ALD film growth *in situ*, as well as to characterize EE-ALD films after FGA by VASE. The M-2000® light source emits a light beam with a known polarization state onto a sample surface at an angle of incidence, θ . The detector then measures the polarization of the reflected light beam in terms of an amplitude ratio, Ψ , and a phase difference, Δ , relative to the incident light beam. Spectroscopic ellipsometry (SE) measures Ψ and Δ for multiple wavelengths, λ , in a specific spectral range.^{31,32}

With the fundamental ellipsometry equation, $\rho = \tan \Psi \cdot e^{i\Delta}$, the measured ellipsometric angles, Ψ and Δ , can be converted mathematically into the complex pseudodielectric response function,^{31–33}

$$\langle \epsilon \rangle = \langle \epsilon_1 \rangle + i \cdot \langle \epsilon_2 \rangle = \sin^2 \theta \cdot \left[1 + \tan^2 \theta \cdot \left(\frac{1 - \rho}{1 + \rho} \right)^2 \right]. \quad (3)$$

While the pseudodielectric function $\langle \epsilon \rangle$ considers a multilayer sample in its entirety,³⁴ the dielectric function ϵ is defined for the bulk material only. ϵ is a fundamental macroscopic property that describes the reaction of a system to an external electric field from an incident light wave.³³ This dielectric response function is also known as the permittivity because ϵ describes how much of the electric field is allowed to pass through a medium.

In its complex version ϵ , the real part, ϵ_1 , represents the ability of the electric field to polarize a dielectric medium. The imaginary part, ϵ_2 , represents any energy losses in a conducting or semiconducting medium through electron-photon interactions. For example, free or bound charges can absorb a photon and transition to a higher-energy state. The ϵ_1 and ϵ_2 spectra are consistent with the Kramers–Kronig relationship.^{31,35}

01 November 2023 15:24:00

The $\langle \epsilon_2 \rangle$ spectra contain information about the effective electronic structure of the film-covered surfaces.³⁶ $\langle \epsilon_2 \rangle$ can be observed and interpreted based on physics even without optical modeling.¹⁶ For example, the electrical resistivity, ρ , of conductive thin films can be estimated based on the Drude theory.^{6,35,37} Metal films with good electrical conductivity, or low ρ , typically exhibit a prominent Drude term. In contrast, carbide or oxide films with high ρ may exhibit a much reduced or no Drude term.

During EE-ALD, iSE results were acquired at the end of each purge step, as shown in Fig. 2. $\langle \epsilon_2 \rangle$ spectra were calculated according to Eq. (3) using the CompleteEASE software version 6.57 (J.A. Woollam Co., Inc.). Ψ and Δ spectra were further evaluated using optical modeling in CompleteEASE, as detailed in Sec. III.

Si with native oxide was used as a starting surface for EE-ALD to simplify the SE data interpretation and modeling. Si with a 400 nm thermal oxide was used for resistivity measurements by 4PP. A SiO₂ wafer coupon was also patterned with sputtered titanium (Ti) to demonstrate whether EE-ALD may grow equally on both insulating and conducting substrates.

III. RESULTS AND DISCUSSION

A. EE-ALD thin film growth and composition

Figure 3 displays the Ru layer thickness versus number of EE-ALD cycles at 160 °C. The Ru layer thickness was determined by iSE at the University of Colorado. The reaction sequence was a 5 s Ru(DMBD)(CO)₃ exposure, 30 s N₂ purge, 10 s electron exposure, and 30 s N₂ purge. The Ru film rapidly nucleated on Si with native oxide and grew linearly over 500 EE-ALD cycles. The growth rate was 0.20 Å/cycle. A Drude-Lorentz model fitted the

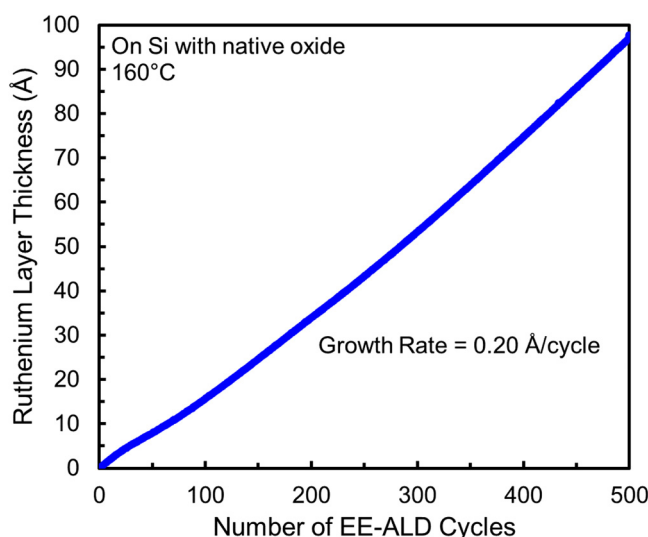


FIG. 3. Ruthenium layer thickness vs number of EE-ALD cycles for Ru EE-ALD on Si with native oxide at 160 °C. Ru film nucleated rapidly and grew without delay at 0.20 Å per cycle. Grid bias was -125 V, and electron current was ~200 mA. Reaction sequence was Ru(DMBD)(CO)₃ exposure for 5 s, purge for 30 s, electron exposure for 10 s, and purge for 30 s.

iSE results with a mean squared error (MSE) of less than 0.4. Slightly enhanced nucleation could result from the difficulties modeling ultra-thin metal films. Slightly enhanced nucleation has been observed in previous EE-ALD experiments.^{5,6}

The deposition temperature of 160 °C was chosen based on results from a previous study of Ru thermal ALD using Ru(DMBD)(CO)₃ and H₂O as the reactants.²¹ 160 °C was the lowest temperature in the ALD window for this Ru thermal ALD process.²¹ This previous study also reported that the DMBD ligand may desorb during Ru(DMBD)(CO)₃ adsorption. DMBD desorption was believed to be similar to DMBD desorption during Si(C₆H₁₀)₂ adsorption on various substrates.³⁸ DMBD desorption would leave only Ru(CO)₃ species on the Ru surface. CO surface species should be desorbed by ESD based on previous ESD studies of CO on Ru(001).³⁹

Figure 4 magnifies the first 10 EE-ALD cycles from Fig. 3 with half-cycle resolution. The Ru layer thickness is plotted after every Ru(DMBD)(CO)₃ and electron exposure indicated by triangle and square symbols, respectively. Nucleation and growth occurred from the first cycle. The Ru layer thickness increased after Ru(DMBD)(CO)₃ exposures. This thickness gain is consistent with the adsorption of Ru(DMBD)(CO)₃ products on the surface. The Ru layer thickness remained relatively constant after subsequent electron exposures. The SE measurements may not be sensitive to the ESD of CO surface species.

The rapid nucleation of this Ru EE-ALD process has significant advantages over the nucleation behavior observed during thermal Ru ALD. Previous *in vacuo* XPS and AFM studies of thermal Ru ALD on hydrogen-terminated silicon, Al₂O₃, and TiN_x surfaces have revealed a smaller initial growth during the nucleation period.¹⁸ There was also a corresponding surface roughness resulting from the incubation period of ~20 ALD cycles. The nucleation regime continued up to 60 ALD cycles before island

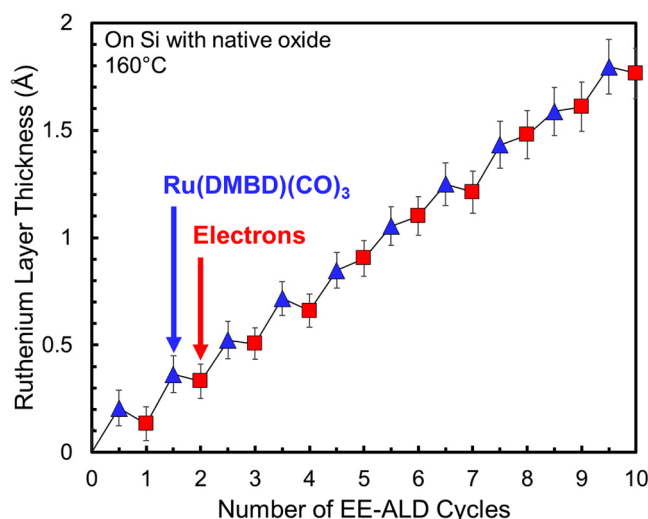


FIG. 4. Magnification of the nucleation regime for Ru EE-ALD in Fig. 3.

coalescence.¹⁸ Other studies of thermal Ru ALD on an insulating SiO₂ surface have revealed an extended incubation period of 40 ALD cycles with virtually no growth. Only minor, isolated RuO_x islands were formed on SiO₂ without any continuous Ru film, especially at lower temperature.¹⁹

The Ru EE-ALD growth rate at 160 °C exhibited self-limiting ALD characteristics at longer Ru(DMBD)(CO)₃ and electron exposures. Figure 5 shows the growth rate versus electron exposure time (square symbols) with the Ru(DMBD)(CO)₃ exposure fixed at 5 s. Figure 5 also displays the growth rate versus Ru(DMBD)(CO)₃ exposure time (triangle symbols) with the electron exposure fixed at 5 s. The two curves did not reach the same saturation value at longer exposure times because a fixed electron exposure of 5 s was undersaturated when varying the Ru(DMBD)(CO)₃ exposure time.

An electron efficiency factor, χ , can be determined from the measured electron current and the Ru growth rate per cycle. This efficiency factor is defined as the number of incident electrons employed per deposited Ru atom in one EE-ALD cycle. Given an electron beam current of ~ 200 mA, the total number of electrons incident on the surface during a 10 s dose is $\sim 1.25 \times 10^{19} \text{ e}^-$. For a Ru growth rate of 0.2 Å/cycle , the number of Ru atoms deposited in the electron irradiated area of 4 cm^2 is $5.815 \times 10^{14} \text{ Ru atoms/cycle}$, assuming a Ru density of 12.2 g/cm^3 and a Ru molar mass of 101.07 g/mol . Consequently, the efficiency factor for Ru EE-ALD under saturation conditions is $\chi = 1.25 \times 10^{19} \text{ e}^- / 5.185 \times 10^{14} \text{ Ru atoms} = \sim 21\,500 \text{ e}^-$ per Ru atom. There are $\sim 21\,500$ electrons incident on the substrate for every deposited Ru atom.

Higher growth rates for Ru electron-enhanced deposition were achieved at lower temperatures. Figure 6 shows the film growth at 60 and 110 °C, using a reaction sequence of 5 s Ru(DMBD)(CO)₃ exposure, 3 s N₂ purge, 10 s electron exposure, and 7 s N₂ purge. At 60 °C with a grid bias voltage of 125 V, the growth rate is

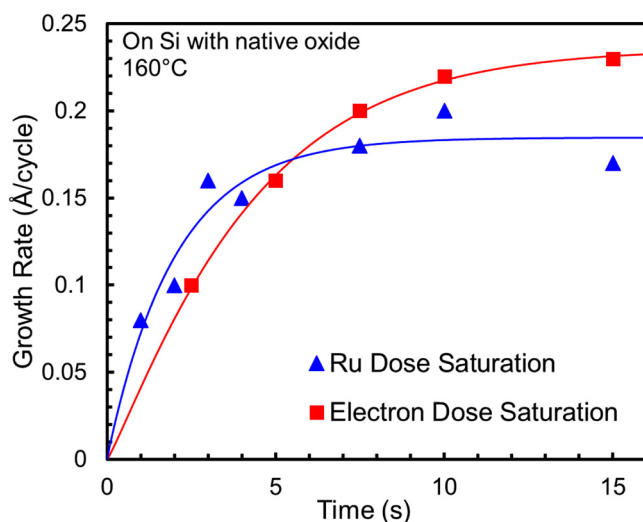


FIG. 5. Self-limiting characteristics of Ru EE-ALD. Ru precursor dose was varied with electron exposures fixed at 5 s. Electron dose was varied with Ru(DMBD)(CO)₃ exposures fixed at 5 s.

$>5 \text{ Å/cycle}$ in zone (A). No electron beam was incident from the HC-PES when the grid bias voltage was set to 0 V. As expected for no electron exposure, no growth was observed in zone (B) at 110 °C. There is also very little CO desorption from the Ru surface at CO coverages $<0.33 \text{ ML}$ at 110 °C during the timescale of the EE-ALD experiments.^{28–30} In contrast, with a grid bias voltage of -125 V , the growth rate is 0.85 Å/cycle at 110 °C in zone (C).

Ru deposition experiments at 60 and 110 °C exhibited higher growth rates than Ru EE-ALD at 160 °C. These higher growth rates are attributed to the non-self-limiting adsorption of more Ru(DMBD)(CO)₃ at lower temperatures and the subsequent decomposition of the Ru(DMBD)(CO)₃ adsorbed species during electron exposures. The resulting Ru films likely contained more carbon impurities. In addition, Ru films deposited at room temperature exhibited optical interference patterns indicating a transparent, nonmetallic film. This temperature dependent behavior is in marked contrast with the temperature dependence of thermal Ru ALD using Ru(DMBD)(CO)₃ and H₂O.²¹ Thermal Ru ALD displays a large reduction in the growth rate for temperatures below 160 °C.²¹

The composition of the as-deposited EE-ALD films was investigated with XPS. An Ru EE-ALD film with a thickness of 18 nm was grown on a Si substrate with native oxide at 160 °C. The reaction sequence was a 5 s Ru(DMBD)(CO)₃ exposure, 30 s N₂ purge, 10 s electron exposure, and 30 s N₂ purge. After EE-ALD, the substrate was removed from the reactor and transferred to the XPS instrument. Figure 7 shows the XPS spectra for a surface scan, as well as after sputtering 3 and 6 nm into the Ru EE-ALD film. Oxygen is observed on the Ru surface due to native oxide formation during sample transfer through ambient air. However, after

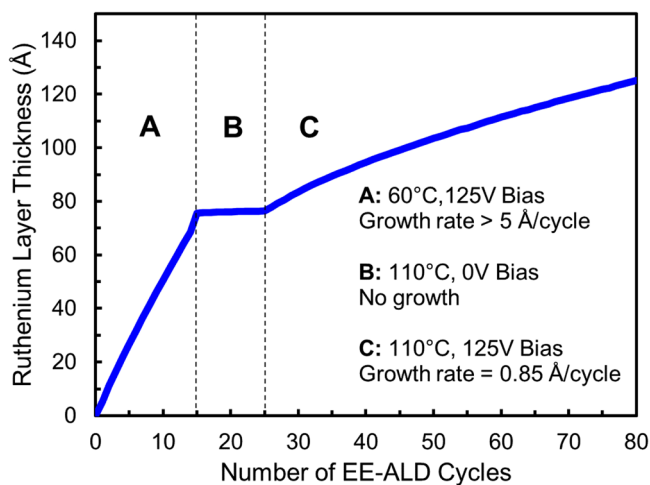


FIG. 6. Ruthenium layer thickness vs number of EE-ALD cycles for Ru EE-ALD at various temperatures and grid bias voltages. Reaction sequence was Ru(DMBD)(CO)₃ exposure for 5 s, purge for 3 s, electron exposure for 10 s, and purge for 7 s: (a) Growth rate of $>5 \text{ Å/cycle}$ at 60 °C with a -125 V grid bias; (b) no growth at 110 °C and 0 V grid bias; and (c) growth rate of 0.85 Å/cycle at 110 °C and -125 V grid bias.

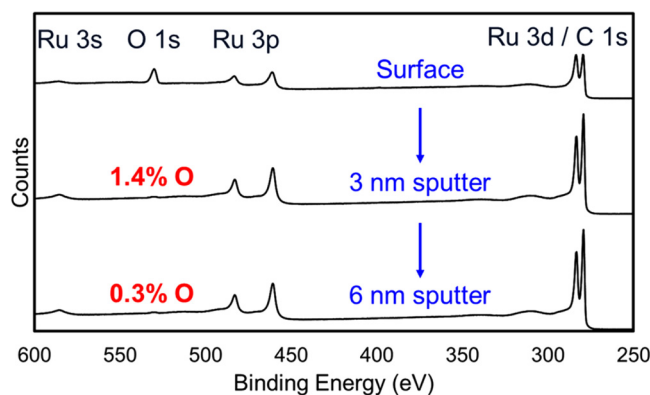


FIG. 7. XPS scans at the surface and after sputtering 3 and 6 nm into an as-deposited EE-ALD film grown at 160 °C. Reaction sequence was Ru(DMBD)(CO)₃ exposure for 5 s, purge for 30 s, electron exposure for 10 s, and purge for 30 s. Negligible oxygen content was revealed in the bulk of Ru EE-ALD films.

sputtering 3 and 6 nm into the film, the oxygen content drops to 1.4 and 0.3 at. %, respectively. These XPS results reveal that the Ru EE-ALD process results in very low oxygen impurities.

In contrast, carbon impurities may be produced during this Ru EE-ALD process. Carbon is difficult to quantify with XPS due to a peak overlap of Ru 3d and C 1s peaks at ~284 eV. However, peak fitting estimations indicated that the as-deposited Ru EE-ALD films could incorporate as much as ~40 at. % C. This carbon could result from DMBD that did not desorb from the Ru surface during Ru(DMBD)(CO)₃ adsorption. Electrons could then decompose the DMBD to leave carbon on the surface. Alternatively, the electrons may not desorb all the adsorbed CO by ESD. Electron dissociation of adsorbed CO could also yield carbon on the surface. However, the low oxygen concentration in the film argues against electron dissociation of CO. Previous experiments for Co EE-ALD using Co(CO)₃NO and electron exposures also deposited Co films with negligible carbon, suggesting no CO electron dissociation.⁴

To test for the electron dissociation of CO, Ru EE-ALD experiments were also conducted using triruthenium dodecacarbonyl [Ru₃(CO)₁₂] as the Ru precursor. The Ru EE-ALD experiments with the Ru₃(CO)₁₂ precursor were performed using the same procedures as the Ru(DMBD)(CO)₃ precursor. The only difference was that the Ru₃(CO)₁₂ precursor was transported into the reaction chamber using a CO carrier gas. As-deposited Ru films grown using Ru₃(CO)₁₂ at room temperature and 100 °C exhibited no Drude term as measured by spectroscopic ellipsometry. In addition, there was no crystallinity measured for the as-deposited Ru films. These results suggest that even in the absence of the DMBD ligand using Ru₃(CO)₁₂, the electrons can dissociate CO and lead to carbon incorporation in the as-deposited Ru films.

B. Forming gas anneal of Ru EE-ALD films

Postdeposition annealing can improve the purity and lower the resistivity, ρ , of Ru EE-ALD thin films.²⁴ A postdeposition forming gas anneal (FGA) consisting of 5% H₂ in 95% N₂ at atmospheric

pressure was performed at 450 °C for 30 min. These experiments were conducted at the University of California San Diego. This FGA significantly affected the as-deposited Ru EE-ALD films.

Figure 8(a) shows the iSE results in the near-infrared (NIR), visible (VIS), and ultraviolet (UV) spectral ranges acquired before and during EE-ALD. This Ru EE-ALD film was grown at 160 °C using a reaction sequence of 5 s Ru(DMBD)(CO)₃ exposure, 30 s N₂ purge, 10 s electron exposure, and 30 s N₂ purge. The starting surface was single-crystalline silicon (Si) with native oxide after pre-heating for 30 min. Figure 8(a) plots the $\langle \epsilon_2 \rangle$ spectrum of this starting surface (thick solid blue line). The transparent NIR region and optical band gap at ~3 eV indicate a semiconducting medium. The characteristic absorption bands at photon energies around 3.4 and 4.2 eV correspond to direct interband transitions of bound charges from the valence to conduction sub-bands in silicon.^{16,36,40,41}

Figure 8(a) then illustrates how the $\langle \epsilon_2 \rangle$ spectra evolved during 1000 Ru EE-ALD cycles. Thin dashed lines are shown for

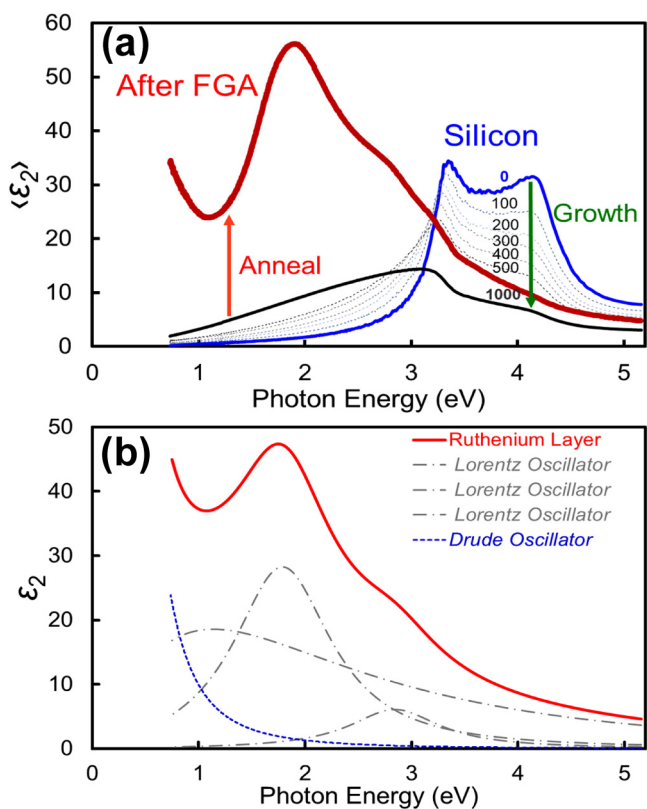


FIG. 8. (a) Measured imaginary part of pseudodielectric function, $\langle \epsilon_2 \rangle$, vs photon energy during 1000 Ru EE-ALD cycles at 160 °C. $\langle \epsilon_2 \rangle$ spectra started from Si with native oxide (thick solid blue line) and evolved with number of EE-ALD cycles. No Drude term was observed during Ru EE-ALD growth. Drude absorption is clearly identified at photon energies below 1 eV after FGA (thick solid red line). (b) Ru bulk model for the Ru EE-ALD film after FGA parameterized with one Drude and three Lorentz oscillators.

100, 200, 300, 400, 500, and 1000 EE-ALD cycles. The Si-characteristic features around 3.4 and 4.2 eV continuously decrease as the growing thin film covers the surface. Meanwhile, new spectral features emerge between 1 and 3 eV. This weak VIS absorption may correspond to electron transitions between the d-bands of Ru.⁴² However, no significant Drude absorption appeared in the NIR region below 1 eV.

The absence of Drude absorption suggested the lack of free charges and the growth of a thin film with low electrical conductivity. This behavior was consistent with the estimated high carbon content of ~40 at. % for the as-deposited EE-ALD film. Carbon contaminants originating from the DMBD or carbonyl ligands may lower the number of conduction electrons available to absorb low-energy photons. An amorphous film would also reduce the mean free path or scattering time, τ , of available electrons.

Figure 8(a) further includes the $\langle \epsilon_2 \rangle$ spectrum of a Ru EE-ALD thin film on Si with native oxide after FGA, measured by VASE (thick solid red line). The annealed film displayed a pronounced transformation: a prominent NIR absorption band emerged at photon energies below 1 eV, signifying an electrically conductive medium. This Drude term corresponds to intraband transitions of free charges as the electron gas of a metal absorbs low-energy photons.

Figure 8(b) plots the optical model according to the VASE results, parameterizing the bulk properties of the Ru layer with one Drude oscillator and three Lorentz oscillators. The following equation describes the shape of the Drude oscillator,^{35,37}

$$\epsilon(E) = \frac{-\hbar^2}{\epsilon_0 \rho (\tau \cdot E^2 + i \hbar E)}. \quad (4)$$

The formation of a prominent Drude absorption indicates that the FGA produces an electrically conductive Ru film. The parameters of the Drude oscillator confirmed a low ρ of $\sim 29 \mu\Omega \cdot \text{cm}$. A relatively long τ of ~ 3 fs suggested rather large crystallites. Strong VIS absorption bands, i.e., Lorentz oscillators, emerged between 1 and 3 eV, corresponding to interband transitions of bound charges between the d-bands of metallic Ru.^{16,42} These observations imply that the FGA removed carbon impurities from the as-deposited Ru EE-ALD film. The individual Drude and Lorentz oscillators in Fig. 8(b) agree well with reported experiment and theory for the Ru bulk.⁴²

The spectra of the Ru EE-ALD film after FGA in Fig. 8 also nearly replicated previous results for thermal Ru ALD.¹⁶ Figure 9 shows the iSE results in the NIR-VIS-UV spectral ranges acquired before and during 150 cycles of thermal Ru ALD. The starting surface was a Si single crystal after native oxide removal (thick solid blue line). The ϵ_2 spectrum of this starting surface exhibited a transparent NIR region, optical band gap around 3 eV, and absorption bands around 3.4 and 4.2 eV, all characteristics of the semiconductor Si.^{16,36,40,41} The $\langle \epsilon_2 \rangle$ spectra then evolved with the number of thermal Ru ALD cycles (thin solid lines).

With a thermal Ru ALD thin film covering the surface, spectral features emerged in the NIR and VIS regions. The formation of a prominent Drude absorption with a low ρ of $\sim 37 \mu\Omega \cdot \text{cm}$ and τ of ~ 2 fs indicates the growth of an electrically conductive,

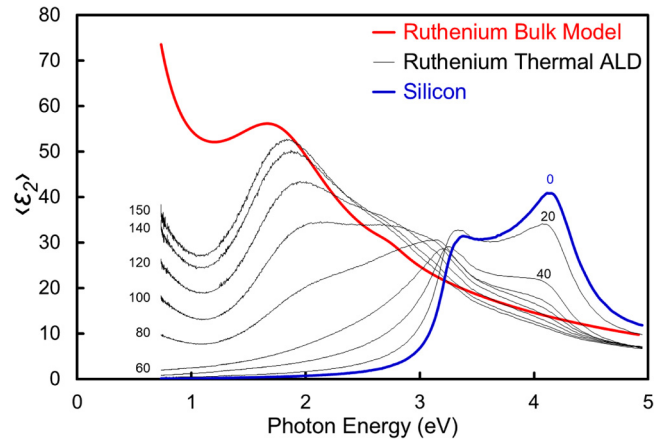


FIG. 9. $\langle \epsilon_2 \rangle$ vs photon energy during 150 cycles of thermal Ru ALD using ECPRu and O_2 at $\sim 275^\circ\text{C}$. $\langle \epsilon_2 \rangle$ spectra started from HF-dipped Si (thick solid blue line) and evolved with number of thermal ALD cycles toward a bulk model of metallic Ru (thick solid red line).

nanocrystalline Ru film. The VIS absorption bands between 1 and 3 eV again correspond to electron transitions between the d-bands of metallic Ru.⁴² The spectrum from the Ru bulk model is also shown for comparison (thick solid red line). The nominal Ru film thickness was 129 Å after 150 thermal ALD cycles, similar to a previous report.¹⁷ 4PP measured a sheet resistance of $19 \Omega/\square$, consistent with a low ρ around $24.6 \mu\Omega \cdot \text{cm}$.

The resistivity of the Ru EE-ALD films was also determined using 4PP (Signatone) measurements. These 4PP measurements require an accurate film thickness to obtain film resistivity. XRR was used to measure the thickness of Ru EE-ALD films deposited on a 400 nm thermal SiO_2 film after FGA. Figure 10(a) displays the XRR scan that obtains a Ru thickness of 6.67 nm for the Ru EE-ALD film after FGA. The thickness determined from XRR measurements was then verified with an AFM line scan. Figure 10(b) shows the AFM line scan that confirms the Ru thickness of 6.86 nm. A set of 10 line scans measured by AFM determines the Ru thickness to be 6.8 ± 0.1 nm.

The XRR thickness was then used in conjunction with the measured sheet resistance to calculate the film resistivity. 4PP was measured near the center of the sample to reduce edge effects. The sheet resistance determined by 4PP was $25.49 \Omega/\square$. The calculated resistivity for the 6.67 nm Ru film was $17.0 \mu\Omega \cdot \text{cm}$ after FGA. This resistivity is consistent with high purity, annealed sputtered Ru films on SiO_2 .²¹

The density of the Ru films was also measured with XRR. The density before FGA was 8.41 g/cm^3 . This density is 68.9% of the bulk Ru density of 12.2 g/cm^3 . In contrast, the density after FGA was 10.99 g/cm^3 . This density is 90.1% of the bulk Ru density. This large density increase is consistent with FGA removing carbon impurities from the as-deposited Ru films. Dense, high purity, and crystalline Ru films are critical to achieving low resistivity.

The effect of the FGA is also evident in the structure of the Ru EE-ALD films. Figure 11 shows the XRD spectra for a Ru EE-ALD

01 November 2023 15:24:00

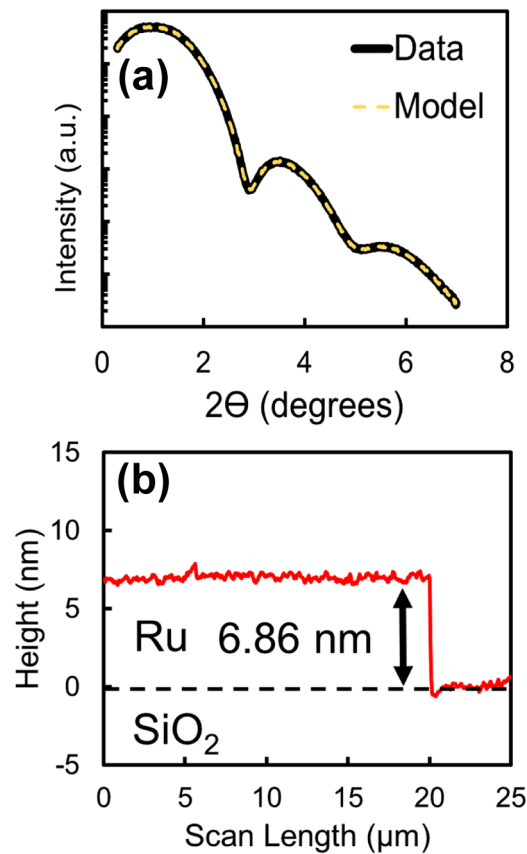


FIG. 10. (a) XRR scan of the Ru EE-ALD film after FGA. Modeling was consistent with a film thickness of 6.67 nm. (b) AFM line scan of Ru EE-ALD film after FGA. Step height yielded a film thickness of 6.86 nm.

film before and after the FGA. Before FGA, Fig. 11(a) revealed no distinguishable peaks in the XRD spectrum, indicating that the film was amorphous. After FGA, Fig. 11(b) revealed diffraction patterns in the XRD spectrum that matched with crystalline metallic Ru. This crystalline Ru film was consistent with removing carbon impurities and a higher purity Ru film with much higher conductivity.

In addition to crystallizing the as-deposited Ru EE-ALD film, the FGA also caused substantial changes to the surface morphology of the Ru EE-ALD films. There was a distinct change in surface roughness measured by AFM before and after the FGA, as shown in Figs. 12(a) and 12(b), respectively. Before FGA, the Ru EE-ALD film was smooth and continuous with an RMS roughness of 0.51 nm. After FGA, the RMS roughness increased to 3.4 nm. The increase in the RMS roughness after FGA is attributed to the crystallization of the Ru film and volume reduction due to carbon removal.

C. Ru EE-ALD films on insulating SiO₂ substrates

Ru EE-ALD films grown on insulating SiO₂ substrates are needed for resistivity measurements. To demonstrate that Ru

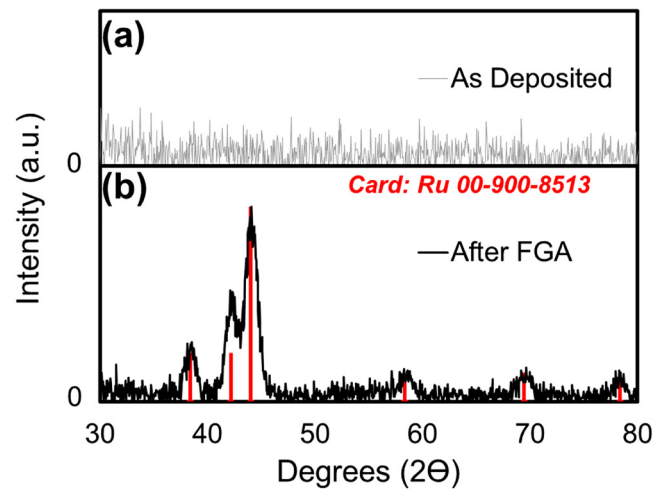


FIG. 11. XRD of the Ru EE-ALD film on Si with native oxide: (a) As-deposited Ru EE-ALD film before FGA; and (b) as-deposited Ru EE-ALD film after FGA. As-deposited Ru EE-ALD film displayed no crystallinity. Ru EE-ALD film was crystalline after FGA.

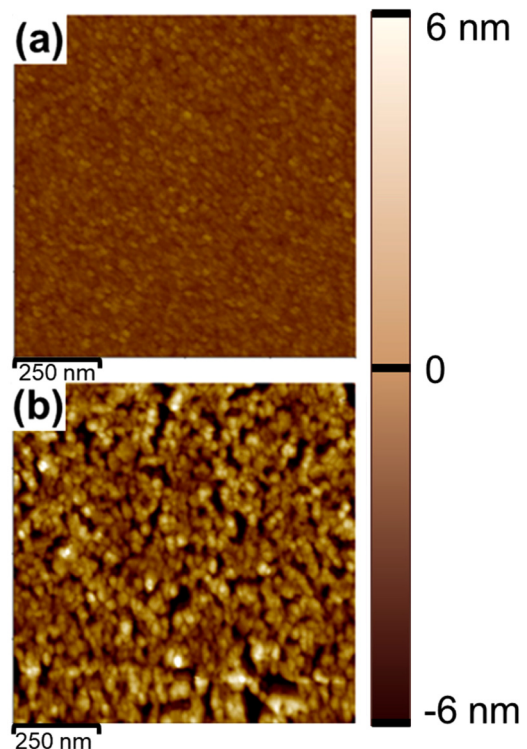


FIG. 12. AFM of Ru EE-ALD film: (a) As-deposited Ru EE-ALD film before FGA; and (b) as-deposited Ru EE-ALD film after FGA. RMS surface roughness increases from 0.51 nm for the as-deposited Ru EE-ALD film to 3.4 nm after FGA.

01 November 2023 15:24:00

EE-ALD can grow on both conductive and insulating substrates, a patterned substrate was created by sputtering a Ti film with a thickness of 35 nm onto a thermal SiO₂ film with a thickness of 400 nm using a shadow mask. The resulting substrate had regions of Ti and regions of SiO₂ on the surface. A Ru EE-ALD film was then grown on this patterned substrate. Based on the previous Ru EE-ALD experiments on conducting samples, this Ru EE-ALD film should have a thickness of 80 nm.

The deposited film was then examined using EDXS with a beam energy of 15 keV. Figure 13 shows elemental maps for Ti, O, Si, and Ru. Figure 13(a) clearly shows the Ti signal on the left-hand side of the sample. Figure 13(b) shows the O signal from the SiO₂ on the right-hand side of the sample. Figure 13(c) displays the Si signal that is more intense on the right-hand side because Ti is not covering the SiO₂ substrate. In contrast, no boundary is visible for the Ru signal shown in Fig. 13(d). This behavior argues that the Ru EE-ALD film grew on both the conductive Ti region and the insulating SiO₂ region of the substrate.

Ru EE-ALD on insulating SiO₂ substrates may be unexpected because the primary electron current could charge the SiO₂ substrate negatively. This negative charge would then establish a negative voltage that would repel additional electron current and prevent EE-ALD. However, if the secondary electron yield from the SiO₂ insulating substrate is greater than unity, the SiO₂ sample would emit more secondary electrons than impinge on the SiO₂ sample from the primary electron beam. These primary and secondary electron fluxes would lead to a positive charge on the insulating SiO₂ sample surface.⁴³

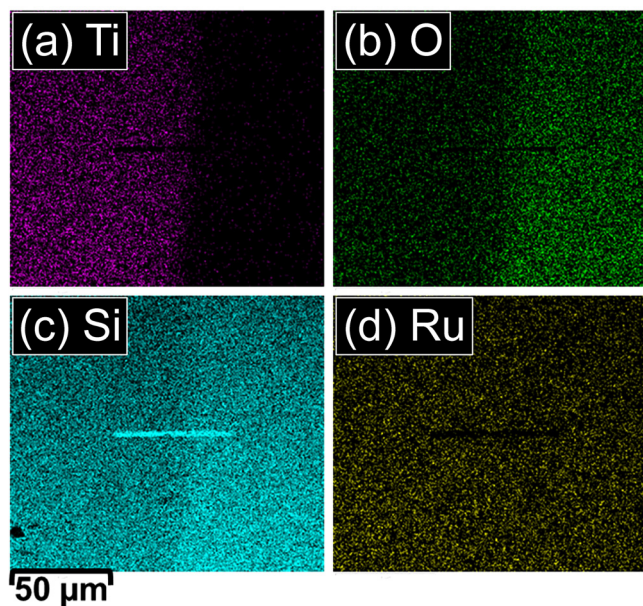


FIG. 13. EDX elemental maps of the Ru EE-ALD film on the Ti(left-hand side)/SiO₂(right-hand side) patterned substrate: (a) Ti; (b) O; (c) Si; and (d) Ru. No boundary is observed for the Ru EDXS signal between Ti(left-hand side) and SiO₂ (right-hand side) regions in (d).

The positive charge on the insulating SiO₂ substrate would create a positive voltage that would pull back secondary electrons.^{43,44} The SiO₂ substrate would charge to a positive voltage where the number of secondary electrons having enough energy to escape would equal the number of incident primary electrons.⁴³ Under these conditions, the EE-ALD could proceed without complication. Only the primary incident electron energy may be increased slightly, resulting from the positive voltage on the SiO₂ substrate.⁴⁴ Measurements for SiO₂ reveal that the secondary electron yield is greater than 1 for primary electron energies from ~100 to 1000 eV.^{45,46} Secondary electron yields greater than unity allow EE-ALD to be performed on SiO₂ and other insulating substrates. Recent experiments for SiO₂ EE-ALD using Si₂H₆, O₃, or H₂O oxygen reactants, and electron exposures are also consistent with EE-ALD on insulating substrates.⁴⁷

D. Ru EE-ALD with reactive background gas

High amounts of carbon impurities were observed in the as-deposited Ru EE-ALD films. No Drude term was observed during the Ru EE-ALD film growth using *in situ* spectroscopic ellipsometry measurements. The as-deposited films also did not display any crystallinity. XPS peak fitting estimated the C content of the as-deposited films to be as high as 40%. The presence of C impurities is also a common observation in the field of focused electron beam induced deposition (FEED).⁴⁸ Design of precursors for FEED is critical to achieve high quality metal deposits.⁴⁹

Recent experiments have demonstrated that reactive background gas (RBG) may be a solution to remove impurities and tune film composition during EE-ALD.⁶ EE-ALD with RBG is a new possibility enabled by the HC-PES.⁶ An RBG at pressures up to ~1 mTorr can be present during the EE-ALD process using the HC-PES as the electron source.⁶ The RBG does not extinguish the HC-PES and does not significantly lower the electron mean free path. With RBG, a wide range of new potential applications for EE-ALD emerge, including reducing oxides, removing carbon impurities, nitridation, oxidation, and carbonization.

This study explored Ru EE-ALD with H₂, NH₃, and H₂O RBGs. These RBGs were selected to try to remove the carbon impurities from the Ru EE-ALD film. $\langle \epsilon_2 \rangle$ spectra from iSE were used as an *in situ* probe to determine the quality of the Ru films deposited with RBG. In particular, the appearance of the Drude peak at <1 eV could assess whether the as-deposited Ru EE-ALD had low resistivity. The goal was to deposit high-conductivity Ru films without requiring FGA.

An electron energy of 125 eV was utilized because electron energies of 75–125 eV generally have high electron impact dissociation or ionization cross sections. At these electron energies, electron impact should generate radical species by dissociating the RBG.⁶ An H₂ RBG should yield H atoms by electron impact dissociation. The H atoms could then remove C impurities from the film as CH₄. The H atoms could also reduce surface oxides by forming H₂O.

Ru EE-ALD films were grown at 160°C using an H₂ RBG. The H₂ (Airgas, 99.999%) gas flow into the reactor was 0.8 SCCM. The H₂ flow was present only during the electron exposure. The H₂ partial pressure during the electron exposure with H₂ RBG was

01 November 2023 15:24:00

2 mTorr. The number of H_2 gas molecules either dissociated or ionized by the electron exposure can be estimated based on the cross section for H_2 electron impact dissociation or ionization and the electron current traveling through the H_2 gas in the volume above the sample.

Electrons can dissociate H_2 into neutral H atoms according to $H_2 \rightarrow H + H$. The cross section for dissociation, σ_d , into neutral H atoms has been measured at electron energies <100 eV. Based on extrapolation from the existing results, $\sigma_d \sim 0.1 \times 10^{-16} \text{ cm}^2$ is estimated at 125 eV.⁵⁰ Electrons can also ionize H_2 according to $H_2 \rightarrow H^+ + H$. The cross section for ionization to produce $H^+ + H$ is $\sigma_{i,H} \sim 0.08 \times 10^{-16} \text{ cm}^2$ at 125 eV.⁵⁰ In addition, the electrons impacting the Ru surface will also produce secondary electrons. The energy of these secondary electrons have a peak at 3–4 eV and a tail stretching out to ~ 40 eV.⁵¹ This tail of the secondary electron

yield could dissociate H_2 because the peak of the H_2 dissociation cross section is $\sigma_d \sim 0.8 \times 10^{-16} \text{ cm}^2$ at 15–20 eV.^{50,52,53}

The Ru EE-ALD film was observed to grow linearly versus EE-ALD cycles with an H_2 RBG. Figure 14(a) shows a linear growth rate of 0.15 Å/cycle during 475 EE-ALD cycles. These results are very similar to the results shown in Fig. 3. Figure 14(b) displays the iSE results during the Ru EE-ALD film growth with H_2 RBG shown in Fig. 14(a). Thin dashed lines are shown for 79, 158, 238, 317, 396, and 475 EE-ALD cycles. Unfortunately, no Drude term was observed in Fig. 14(b) during Ru EE-ALD. This result may indicate that the H atoms could not clean the carbon impurities from the as-deposited Ru EE-ALD film. Perhaps the H atom flux was insufficient to remove the carbon impurities. Ru EE-ALD films deposited with the H_2 RBG were successfully annealed using FGA to remove C impurities and improve the film conductivity.

NH_3 and H_2O were also investigated as RBGs during Ru EE-ALD. NH_3 can provide a flux of NH_2 radicals and H atoms on the surface. H_2O can provide a flux of OH radicals and H atoms on the surface. However, no Drude terms were observed in the iSE results after Ru EE-ALD with NH_3 or H_2O RBGs. These results indicate that the carbon in the Ru film is not easily removed by the flux of radical species from NH_3 or H_2O dissociation.

IV. CONCLUSIONS

Ru EE-ALD was performed using alternating Ru(DMBD)(CO)₃ and electron exposures. A new EE-ALD reactor was constructed by integrating an HC-PES into a hot-wall viscous-flow ALD reactor. Ru films grown with EE-ALD at 160 °C were demonstrated to nucleate rapidly and grow linearly on Si with native oxide. The growth rate for Ru EE-ALD was 0.2 Å/cycle under saturating conditions. Comparing Ru EE-ALD growth on a patterned Ti/SiO₂ surface indicated identical growth on both conductive and insulating substrates. Secondary electron emission that maintains a charge-neutral surface during electron exposures is believed to enable EE-ALD on insulating surfaces.

FGA effectively removed carbon impurities from the Ru EE-ALD film and improved the film resistivity. The Ru thickness of 6.8 ± 0.1 nm after FGA was measured with XRR and confirmed with an AFM line scan. Ru resistivity calculated from the measured thickness and sheet resistance was $17.0 \mu\Omega \text{ cm}$. This low resistivity is consistent with annealed sputtered Ru films of similar thickness. XRD also observed crystalline Ru after FGA. In addition, the increase in the surface roughness after FGA was attributed to a crystallized Ru film.

SE was used to monitor the thin film growth during EE-ALD. When $\langle \epsilon_2 \rangle$ spectra reveal an absorption of low-energy photons, this Drude term is directly proportional to the number of free electrons of a conductive medium. For the Ru EE-ALD films, the Drude term was apparent only after FGA. This behavior indicates that the FGA effectively removed carbon impurities and created a high-conductivity metallic Ru film.

Various RBGs were explored during the EE-ALD process in an attempt to remove the carbon impurities without performing the FGA. Ru EE-ALD was conducted in the presence of H_2 , NH_3 , and H_2O RBGs. Unfortunately, iSE measurements during Ru

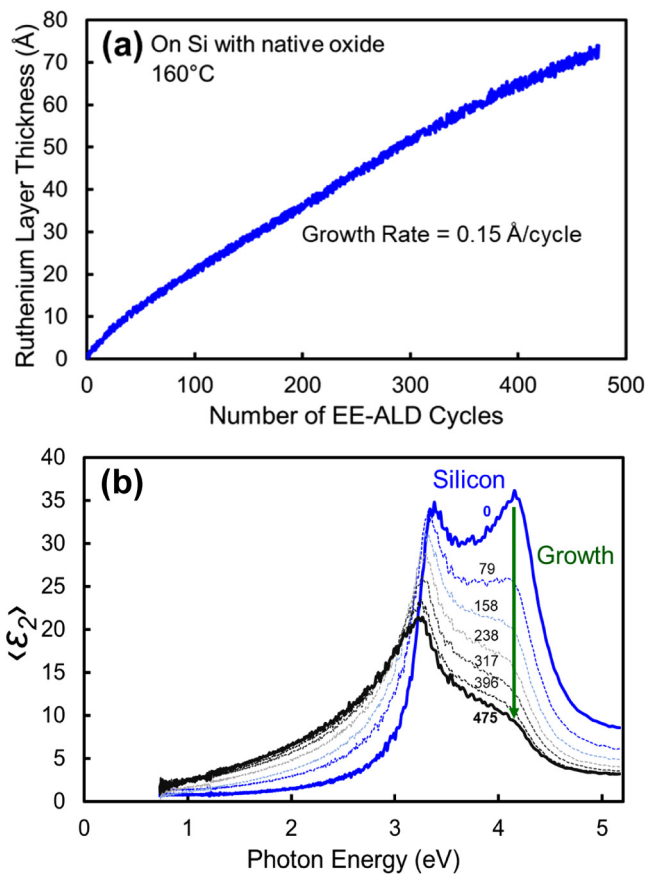


FIG. 14. (a) Ruthenium layer thickness vs number of Ru EE-ALD cycles with H_2 RBG on Si with native oxide at 160 °C. Grid bias was -125 V, and electron current was 200 mA. Ru layer thickness immediately nucleated and grew with number of EE-ALD cycles at 0.15 Å per cycle during 475 EE-ALD cycles. (b) $\langle \epsilon_2 \rangle$ vs photon energy during Ru EE-ALD with H_2 RBG as shown in (a). No Drude term was observed at low photon energies indicating that H_2 RBG did not sufficiently remove carbon impurities.

01 November 2023 15:24:00

EE-ALD with H_2 , NH_3 , and H_2O RBGs did not reveal any Drude term. These results indicated that the RBG could not easily remove the carbon impurities from the Ru EE-ALD films.

ACKNOWLEDGMENTS

This work was supported by the Joint University Microelectronics Program (JUMP), funded by the Semiconductor Research Corporation (SRC). The authors thank Ravi Kanjolia and Mansour Moinpour from EMD Performance Materials for supplying the $\text{Ru}(\text{DMBD})(\text{CO})_3$ precursor. The authors thank Tomoko Borsa of the Colorado Shared Instrumentation in Nanofabrication and Characterization (COSINC) for obtaining the SEM/EDXS images. The authors also thank Kenneth Smith and Don David from the University of Colorado Integrated Instrument Development Facility for constructing the HC-PES and computer interfacing.

AUTHOR DECLARATIONS

Conflict of interest

The authors have no conflicts to disclose.

Author Contributions

Michael A. Collings: Conceptualization (supporting); Data curation (lead); Formal analysis (lead); Investigation (lead); Methodology (supporting); Writing – original draft (lead); Writing – review & editing (supporting). **Marcel Junige:** Data curation (supporting); Formal analysis (supporting); Investigation (supporting); Methodology (supporting); Writing – original draft (supporting); Writing – review & editing (supporting). **Andrew S. Cavanagh:** Data curation (supporting); Resources (lead). **Victor Wang:** Data curation (supporting); Methodology (supporting); Resources (supporting). **Andrew C. Kummel:** Methodology (supporting); Resources (supporting); Supervision (supporting). **Steven M. George:** Conceptualization (lead); Funding acquisition (lead); Methodology (lead); Project administration (lead); Supervision (lead); Writing – review & editing (lead).

DATA AVAILABILITY

The data that support the findings of this study are available within the article.

REFERENCES

- ¹J. K. Sprenger, A. S. Cavanagh, H. Sun, K. J. Wahl, A. Roshko, and S. M. George, *Chem. Mater.* **28**, 5282 (2016).
- ²J. K. Sprenger, H. Sun, A. S. Cavanagh, and S. M. George, *J. Vac. Sci. Technol. A* **36**, 01A118 (2018).
- ³J. K. Sprenger, H. Sun, A. S. Cavanagh, A. Roshko, P. T. Blanchard, and S. M. George, *J. Phys. Chem. C* **122**, 9455 (2018).
- ⁴Z. C. Sobell, A. S. Cavanagh, and S. M. George, *J. Vac. Sci. Technol. A* **37**, 060906 (2019).
- ⁵Z. C. Sobell, A. S. Cavanagh, D. R. Boris, S. G. Walton, and S. M. George, *J. Vac. Sci. Technol. A* **39**, 042403 (2021).
- ⁶Z. C. Sobell and S. M. George, *Chem. Mater.* **34**, 9624 (2022).
- ⁷S. M. George, *Chem. Rev.* **110**, 111 (2010).
- ⁸R. D. Ramsier and J. T. Yates, *Surf. Sci. Rep.* **12**, 246 (1991).

- ⁹F. Bozso and P. Avouris, *Phys. Rev. B* **38**, 3943 (1988).
- ¹⁰J. W. Elam, M. D. Groner, and S. M. George, *Rev. Sci. Instrum.* **73**, 2981 (2002).
- ¹¹M. Junige and S. M. George, *J. Vac. Sci. Technol. A* **39**, 023204 (2021).
- ¹²D. Gall, *J. Appl. Phys.* **127**, 050901 (2020).
- ¹³T. Aaltonen, P. Alén, M. Ritala, and M. Leskelä, *Chem. Vap. Deposition* **9**, 45 (2003).
- ¹⁴T. Aaltonen, A. Rahtu, M. Ritala, and M. Leskelä, *Electrochem. Solid-State Lett.* **6**, C130 (2003).
- ¹⁵K. Kukli *et al.*, *J. Electrochem. Soc.* **158**, D158 (2011).
- ¹⁶M. Junige, M. Geidel, M. Knaut, M. Albert, and J. W. Bartha, “Monitoring atomic layer deposition processes in situ and in real-time by spectroscopic ellipsometry,” in *2011 Semiconductor Conference Dresden*, Dresden, Germany, 27–28 September 2011 (IEEE, Dresden, 2011), p. 1.
- ¹⁷M. Knaut, M. Junige, M. Albert, and J. W. Bartha, *J. Vac. Sci. Technol. A* **30**, 1 (2012).
- ¹⁸M. Geidel, M. Junige, M. Albert, and J. W. Bartha, *Microelectron. Eng.* **107**, 151 (2013).
- ¹⁹M. Junige, M. Löffler, M. Geidel, M. Albert, J. W. Bartha, E. Zschech, B. Rellinghaus, and W. F. V. Dorp, *Nanotechnology* **28**, 395301 (2017).
- ²⁰S. Killge *et al.*, *Microelectron. Eng.* **205**, 20 (2019).
- ²¹Z. Gao, D. Le, A. Khaniya, C. L. Dezelah, J. Woodruff, R. K. Kanjolia, W. E. Kaden, T. S. Rahman, and P. Banerjee, *Chem. Mater.* **31**, 1304 (2019).
- ²²M. Breeden, V. Wang, R. Kanjolia, M. Moinpour, J. Woodruff, H. Simka, and A. Kummel, “Ru ALD With Bulk-Like Resistivity for Interconnects,” in *2022 IEEE International Interconnect Technology Conference (IITC)*, San Jose, CA, 27–30 June 2022 (IEEE, 2022), p. 120.
- ²³D. Z. Austin, M. A. Jenkins, D. Allman, S. Hose, D. Price, C. L. Dezelah, and J. F. Conley, Jr., *Chem. Mater.* **29**, 1107 (2017).
- ²⁴M. Hayes, M. A. Jenkins, J. Woodruff, D. F. Moser, C. L. Dezelah, and J. F. Conley, Jr., *J. Vac. Sci. Technol. A* **39**, 052402 (2021).
- ²⁵S. Cwik, K. N. Woods, M. J. Saly, T. J. Knisley, and C. H. Winter, *J. Vac. Sci. Technol. A* **38**, 012402 (2020).
- ²⁶M. T. Postek, W. J. Keery, and R. D. Larrabee, *Scanning* **11**, 111 (1989).
- ²⁷J. R. Schneider, C. de Paula, J. Lewis, J. Woodruff, J. A. Raiford, and S. F. Bent, *Small* **18**, 2105513 (2022).
- ²⁸J. L. Brand, M. V. Arena, A. A. Deckert, and S. M. George, *J. Chem. Phys.* **92**, 4483 (1990).
- ²⁹A. A. Deckert, J. L. Brand, M. V. Arena, and S. M. George, *Surf. Sci.* **208**, 441 (1989).
- ³⁰H. Pfnur, P. Feulner, and D. Menzel, *J. Chem. Phys.* **79**, 4613 (1983).
- ³¹H. Fujiwara, *Spectroscopic Ellipsometry: Principles and Applications* (John Wiley & Sons, Ltd., Chichester, UK, 2007).
- ³²H. G. Tompkins and E. A. Irene, *Handbook of Ellipsometry* (William Andrew Inc., Norwich, NY, 2005), ISBN: 978-0-8155-1499-2.
- ³³H. Kuzmany, *The dielectric function*, in *Solid-State Spectroscopy: An Introduction* (Springer, Berlin, 1998), p. 101.
- ³⁴J. N. Hilfiker, N. Singh, T. Tiwald, D. Convey, S. M. Smith, J. H. Baker, and H. G. Tompkins, *Thin Solid Films* **516**, 7979 (2008).
- ³⁵J. N. Hilfiker and T. Tiwald, “Dielectric function modeling,” in *Spectroscopic Ellipsometry for Photovoltaics: Fundamental Principles and Solar Cell Characterization*, edited by H. Fujiwara, R. W. Collins (Springer Cham, Springer, Cham, Switzerland, 2018), Vol. 1, p.115.
- ³⁶P. Lautenschlager, M. Garriga, L. Vina, and M. Cardona, *Phys. Rev. B* **36**, 4821 (1987).
- ³⁷T. E. Tiwald, D. W. Thompson, J. A. Woollam, W. Paulson, and R. Hance, *Thin Solid Films* **313–314**, 661 (1998).
- ³⁸C.-M. Chiang, J. E. Rowe, R. A. Malic, A. Sen, M. L. Steigerwald, and A. P. Mills, *Appl. Surf. Sci.* **107**, 189 (1996).
- ³⁹P. Feulner, H. A. Engelhardt, and D. Menzel, *Appl. Phys.* **15**, 355 (1978).
- ⁴⁰G. E. Jellison and F. A. Modine, *Phys. Rev. B* **27**, 7466 (1983).
- ⁴¹G. E. Jellison and F. A. Modine, *J. Appl. Phys.* **76**, 3758 (1994).
- ⁴²W. S. Choi, S. S. A. Seo, K. W. Kim, T. W. Noh, M. Y. Kim, and S. Shin, *Phys. Rev. B* **74**, 205117 (2006).

- ⁴³H. J. Hopman, H. Alberda, I. Attema, H. Zeijlemaker, and J. Verhoeven, *J. Electron. Spectrosc. Relat. Phenom.* **131–132**, 51 (2003).
- ⁴⁴J. Cazaux, P. Lehuède, and J. Electron, *J. Electron Spectrosc. Relat. Phenom.* **59**, 49 (1992).
- ⁴⁵G. F. Dionne, *J. Appl. Phys.* **46**, 3347 (1975).
- ⁴⁶J. J. Fijol, A. M. Then, G. W. Tasker, and R. J. Soave, *Appl. Surf. Sci.* **48–49**, 464 (1991).
- ⁴⁷J. C. Gertsch, Z. C. Sobell, A. S. Cavanagh, H. Simka, and S. M. George, *J. Vac. Sci. Technol. A* **41**, 042404 (2023).
- ⁴⁸J. J. L. Mulders, *Nanofabrication* **1**, 74 (2014).
- ⁴⁹A. Mahgoub, H. Lu, R. M. Thorman, K. Preradovic, T. Jurca, L. McElwee-White, H. Fairbrother, and C. W. Hagen, *Beilstein J. Nanotechnol.* **11**, 1789 (2020).
- ⁵⁰J.-S. Yoon, M.-Y. Song, J.-M. Han, S.-H. Hwang, W.-S. Chang, B. Lee, and Y. Itikawa, *J. Phys. Chem. Ref. Data* **37**, 913 (2008).
- ⁵¹H. Seiler, *J. Appl. Phys.* **54**, R1 (1983).
- ⁵²S. Chung, C. C. Lin, and E. T. P. Lee, *Phys. Rev. A* **12**, 1340 (1975).
- ⁵³S. J. B. Corrigan, *J. Chem. Phys.* **43**, 4381 (1965).